

# Reconstruction from a flexible number of projections in cone-beam computed tomography via active shape models

Peter B. Noël<sup>a,b</sup>, Jason J. Corso<sup>a</sup>, Jinhui Xu<sup>b</sup>, Kenneth R. Hoffmann<sup>a,b</sup>, Sebastian Schafer<sup>b</sup>  
and Alan M. Walczak<sup>b</sup>

<sup>a</sup>Department of Computer Science and Engineering, The State University of New York at Buffalo, USA.

<sup>b</sup>Department of Neurosurgery (Toshiba Stroke Research Center), The State University of New York at Buffalo, USA.

## ABSTRACT

With a steady increase of CT interventions, population dose is increasing. Thus, new approaches must be developed to reduce the dose. In this paper, we present a means for rapid identification and reconstruction of objects of interest in reconstructed data. Active shape models are first trained on sets of data obtained from similar subjects. A reconstruction is performed using a limited number of views. As each view is added, the reconstruction is evaluated using the active shape models. Once the object of interest is identified, the volume of interest alone is reconstructed, saving reconstruction time. Note that the data outside of the objects of interest can be reconstructed using fewer views or lower resolution providing the context of the region of interest data. An additional feature of our algorithm is that a reliable segmentation of objects of interest is achieved from a limited set of projections. Evaluations were performed using simulations with Shepp-Logan phantoms and animal studies. In our evaluations, regions of interest are identified using about 33 projections on average. The overlap of the identified regions with the true regions of interest is approximately 91%. The identification of the region of interest requires about 1/5 of the time required for full reconstruction, the time for reconstruction of the region of interest is currently determined by the fraction of voxels in the region of interest (i.e, voxels in region of interest/voxels in full volume). The algorithm has several important clinical applications, e.g., rotational angiography, digital tomosynthesis mammography, and limited view computed tomography.

## 1. INTRODUCTION

In recent years, cone beam computed tomography (CBCT) has been used more frequently in the clinical arena. During these interventions, many situations arise where only a sparse segmentation of the object of interest would be useful within a short timeframe. Therefore, it is of interest to minimize the number of projections which are necessary to reliably reconstruct objects of interest. This unique situation enables us to focus on objects and regions of interest.

In other situations, only a limited set of projections is available, but a reliable reconstruction is needed; some examples include cardiac CT, where the motion of the heart limits the number of views that can be used, and applications where one cannot traverse completely around the object due to mechanical limitations. Note, a lower number of views also reduces the radiation dose to the patient.

Several groups have recently worked on the limited view reconstruction problem. State of the art techniques for limited view reconstruction (backprojection method, simultaneous algebraic reconstruction technique, and maximum likelihood method) are revisited by Zhang, et al.<sup>1</sup> Experimental results showing the tradeoff between completion and the noise level of reconstruction are in Chen, et al.<sup>2</sup> A theoretical framework for reconstruction from highly incomplete data is given in Candes, et al.<sup>3</sup> A new denoising algorithm for limited view reconstructions is presented in Singh, et al.<sup>4</sup>

In our case, we make use of prior knowledge. Compared to the approaches when the lower number of projection is determined independent of the object of interest, we determine the necessary number of projection

---

Further author information: (Send correspondence to Peter B. Noël)  
Peter B. Noël: E-mail: pbnoel@buffalo.edu, Telephone: (716) 829-3594

by using prior knowledge of the objection of interest. Our method rapidly identifies a volume of interest using active shape models<sup>5</sup> while reconstructing from a flexible number of projections. The volume of interest can be subsequently reconstructed by using the full projection set. If necessary the volume of interest can then be reconstructed more quickly and with improved statistics. An additional feature of our algorithm is that a segmentation of objects of interest is done from a limited set of projections.

## 2. METHOD

In our approach, active shape models are trained to identify pre-specified objects in the images. Then, limited view reconstructions are performed using progressively more views. After each reconstruction, active shape models are used to identify, if possible, objects of interest. Views continue to be added until the object of interest is identified. Once identified, the segmentation of the object of interest is returned. Or the object of interest is reconstructed using all projection data. Regions outside the object of interest can be identified using limited view or lower resolution techniques.

### 2.1 Cone-Beam Computed Tomography (CBCT)

In this section, we revisit a reconstruction method for CBCT data as introduced by Feldkamp et al.<sup>6</sup> Since we use a rotational angiographic system equipped with a flat panel detector, we only discuss the case of equally spaced planar detectors.

In figure 1, the schematic drawing of the cone beam system with a planar detector is presented. During acquisition the system follows a circular trajectory, with a radius of  $D$  placed at the origin. The detector plane lies perpendicular to the central axis of the x-ray beam.

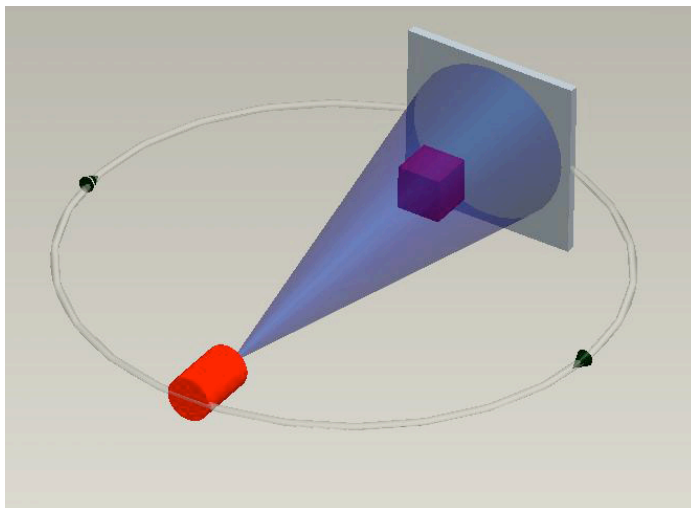


Figure 1. Systematic drawing of the cone beam system. The gantry rotates about the patient.

The projection image  $P(\cdot)$  at angular position  $\Theta$  is the line integral along the x-ray beam. A set of projections are acquired at  $t$  discrete source positions with uniform angular spacing  $\Delta\Theta$ . During CBCT,  $\Theta$  range is about  $210^\circ$  with angular separations of  $1^\circ$ . A full rotation is not possible due to mechanical limitations.

The reconstruction method is formulated as a weighted filtered backprojection. As an initial step, the projection data are log converted, individually weighted and ramp filtered ( $P_f$ ). Next, the 3-D volume is reconstructed by a backprojection. Let  $r = [x, y, z]$  be the 3-D position in the volume, and let  $(u, v)$  denote the position of the intersection with the detector plane of the ray starting from the source and passing through point  $r$ . Therefore, the reconstruction of the value  $f(r)$  is given by:

$$f(\vec{r}) = \sum_{\Theta} P_f[u(x, y, \Theta), v(x, y, \Theta), \Theta], \quad (1)$$

where

$$u = (SID * x)/(ISO - z), \quad (2)$$

$$v = (SID * y)/(ISO - z), \quad (3)$$

SID is the source-to-image-distance, and ISO is the isocenter distance. The isocenter is the point about which the system rotates, and the isocenter distance is the source-to-isocenter-distance. Since  $u$  and  $v$  usually do not correspond to a discrete pixel position, we use interpolation to determine the corresponding gray value in the image. The computational cost of cone-beam computed tomography for a volume of size  $N^3$  is  $O(N^4)$ .

Additionally to improve our technique, we have implemented the filtered backprojection algorithm for 3-D reconstruction of CBCT data using the Compute Unified Device Architecture (CUDA) provided by NVIDIA (NVIDIA Cor., Santa Clara, California), which was executed on a NVIDIA GeForce 280 GTX.<sup>7</sup> Our implementation results in improved reconstruction times from on the order of minutes, and perhaps hours, to a matter of seconds.

Rather than using the standard reconstruction approach, we monitor the reconstruction progress by using active shape models. We review next the active shape models before introducing our full approach.

## 2.2 Active Shape Models (ASMs)

Different types of prior shape models are available, but one of the most popular ones is Active Shape Models (ASMs), because of its robustness and ability to capture more than one structure in a scene.

In our implementation, we use the ASMs as described by Cootes et al.<sup>5</sup> which uses point-distribution models (PDMs). PDMs are a set of  $n$  landmarks, where each training sample is a  $d$ -dimensional vector of landmarks. All training samples are aligned in a least square sense by using the Procrustes algorithm.<sup>8</sup> The differences between the mean shape and the aligned shapes are the vectors which form the columns of the landmark configuration matrix  $L$ . We determine the principle modes of variation in the training data by applying principal component analysis (PCA) to the configuration matrix  $L$ . By using only the first  $c$  modes all valid shapes ( $x$ ) can be represented by:

$$x = \bar{x} + Qb \quad (4)$$

where  $\bar{x}$  is the mean shape,  $Q$  is the matrix of the first  $c$  eigenvectors and  $b$  is a vector of weights also called the shape parameters.

To define the limits on valid shapes, the range of each shape parameter  $b_i$  is:

$$-3\sqrt{\lambda_i} \leq b_i \leq 3\sqrt{\lambda_i} \quad (5)$$

where  $\lambda_i$  is the  $i$ th eigenvalue of the configuration matrix. Shapes having all  $b_i$  within this limits are considered to be valid. A found shape in the unknown image with  $dx$  relative to  $\bar{x}$  can be validated by:

$$db = Q^T dx \quad (6)$$

In figure 2, we show an example for the ASMs where the algorithm is trying to find a C-arm gantry in the scene (given as a toy example). Note, this takes less than one second on a standard PC.

## 2.3 Reconstruction by using Priors

We present the basic flow chart of our algorithm in figure 3. As an initial step, we train the ASMs for the objects of interest that we expect to be reconstructing later (these can be any anatomical shape). The training is done as described earlier by using PDMs.

Next, we start to reconstruct (section 2.1) using  $n$  randomly chosen projections. By picking the projections randomly, we are able to obtain image information earlier in the volumetric data. This is true since a projection contains more information relative to a second projection if the angular distances between the projection is larger than the standard one degree. In the next step, we apply the trained ASM to our approximated volumetric data. The mean shape is placed at the center of mass of the training data. The landmark points from  $\bar{x}$  move along the gradient of the volume. The returned  $dx$  from this procedure is then validated by equation (6). In the case where no valid shape was found, a single random projection is added to our reconstruction. Basically, the algorithm adds new information to the intermediate result until this process converges and a valid shape is found.

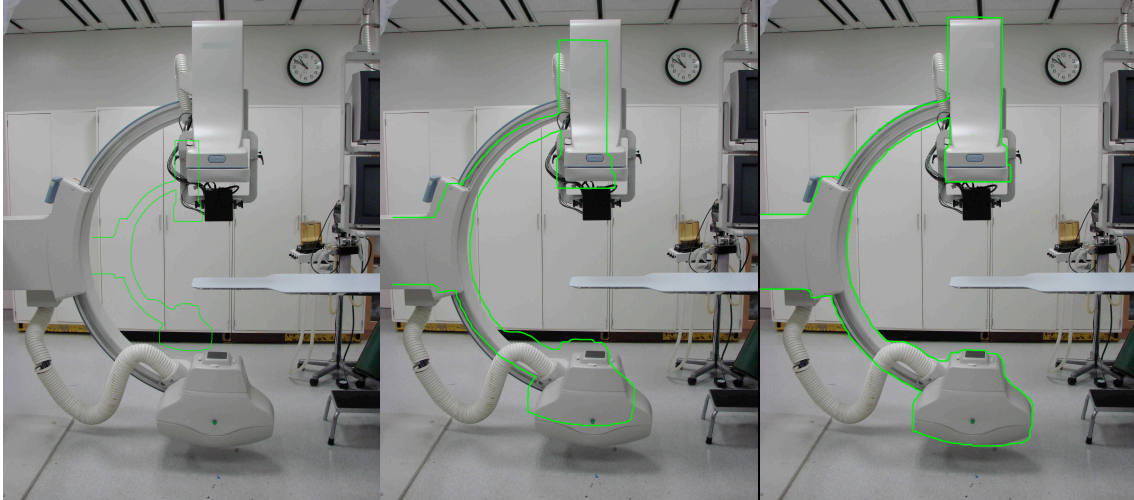


Figure 2. Example for ASMs, trying to find the gantry in the scene. Initial pose (left), after several iterations (middle), and convergence (right). Note, this is only an example to show the ASM results.

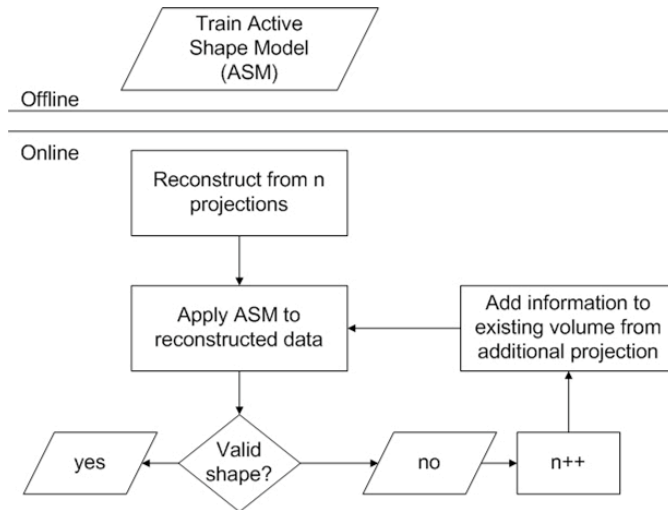


Figure 3. Illustration of our combined algorithm of filtered backprojections and ASMs.

## 2.4 Errors and Limitations

To achieve good results, training points (landmarks) should be placed relatively accurately during training (to within a few pixels), to optimally capture the shape of the object of interest. The accuracy of the training points reduces the influence of the terms describing the noise caused by errors in the point locations. Even if the algorithm does not converge, all projection data will eventually be included in the reconstruction. This may happen if no instance of the model is found in the scene. Note, this situation never happened during our evaluation.

## 3. EVALUATIONS

We evaluated our algorithm on simulated and actual CBCT data.

For the simulations, we use the standard Shepp-Logan phantom which was generated using Matlab. The phantom data were reprojected into 360 views (SID 123, ISO 82), with an angular separation of  $1^\circ$ . As a preprocessing step, we train our ASM on landmark points labeled in the original image. To add variation to our landmark points, we add random noise to each landmark point ( $\pm 4$  pixel), to simulate 10 different sample arrangements for training.

In order to determine the performance of our algorithm on real data, we use data from a rabbit study. The CBCT system (Toshiba Infinix VSI/02) acquires 106 projections with an angular separation of  $2^\circ$  and a matrix size of  $1024 \times 1024$ . The projections were not distortion corrected since our system is equipped with a flat panel detector. We evaluated our technique using a cross-validation/leave-one-out procedure by using ten clinical cases. For each training set, we iteratively leave one example out and compute a reconstruction on the remaining examples. For the left out data set, the number of necessary projections ( $t_{\#P}$ ) and the percent error in overlap between the manually indicated area and the resulting area ( $E_a$ ) is computed. In this study, we chose as a anatomic structure (volume of interest) the lower jaw of the rabbit.

#### 4. RESULTS

Figure 4 shows a slice from our reconstruction and segmentation achieved using our algorithm. The objects were reliably identified in the reconstruction using only 16 random projections

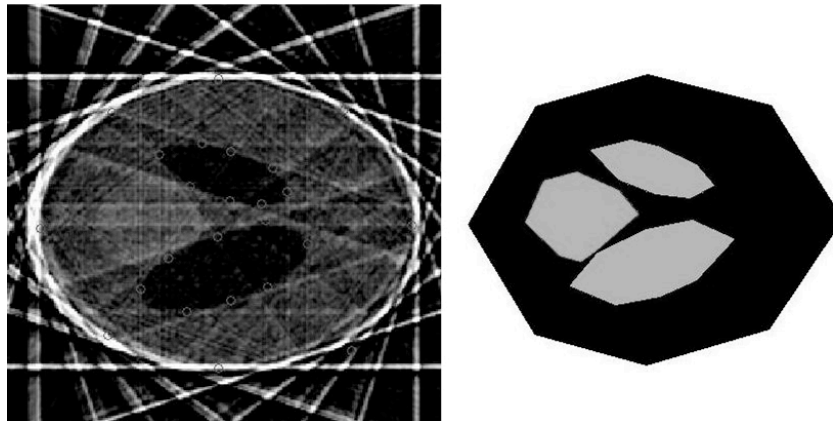


Figure 4. The sparse reconstruction after using 16 projection (left) and the corresponding segmentation (right). Note, the reliable segmentation after a limited super of projection is an additional feature of our algorithm.

Table 1 presents the results of our cross-validation from an animal study. The number of necessary projections  $t_{\#P}$  returned from our algorithm ranges between 25 and 41. These differences may be caused from the variation of the quality of the projections and of the surrounding area of the object of interest. The error,  $E_a$ , (the average percent difference in overlap between manually indicated and resulting area) is approximately 9%.

Table 1. Results from the cross-validation

	$t_{\#P}$	$E_a$ (%)
case 1	31	9
case 2	27	11
case 3	41	5
case 4	33	8
case 5	39	13
case 6	35	10
case 7	41	7
case 8	25	9
case 9	32	12
case 10	30	7

In Figure 5, we present the results of the reconstruction. Our algorithm was able to detect the lower jaw after reconstruction from 31 randomly picked projections. To evaluate our technique, we compared the segmented area returned after 31 projections with the manually indicated area in the full reconstruction (106 projection). The average overlap of the two areas was 91%.

The full reconstruction of the volume of interest is illustrated in Figure 6. In this case, we focus on the full body of the rabbit. Comparing our result with the standard reconstruction, we found no loss of information in the volume of interest. However, the time needed to reconstruct is reduced by a factor of approximately 2.

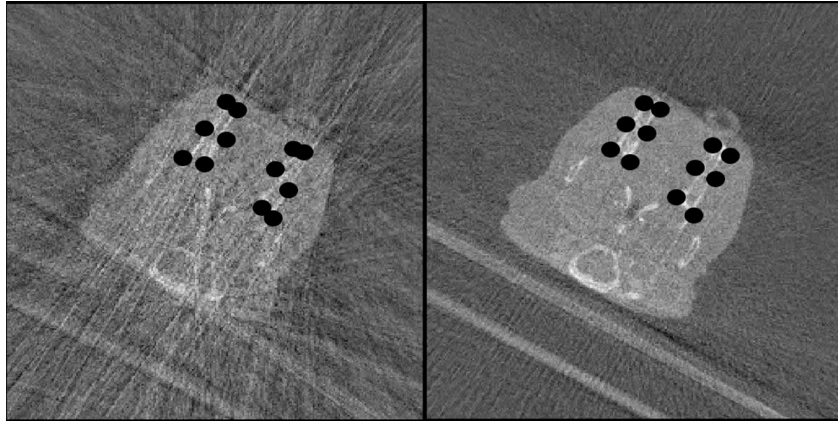


Figure 5. The sparse reconstruction returned by our algorithm after 31 projections (left), the full reconstruction of the corresponding slices (right). The landmark points are shown as black dots. Note, our algorithm was able to detect similar landmark points by using only a low number of projections.

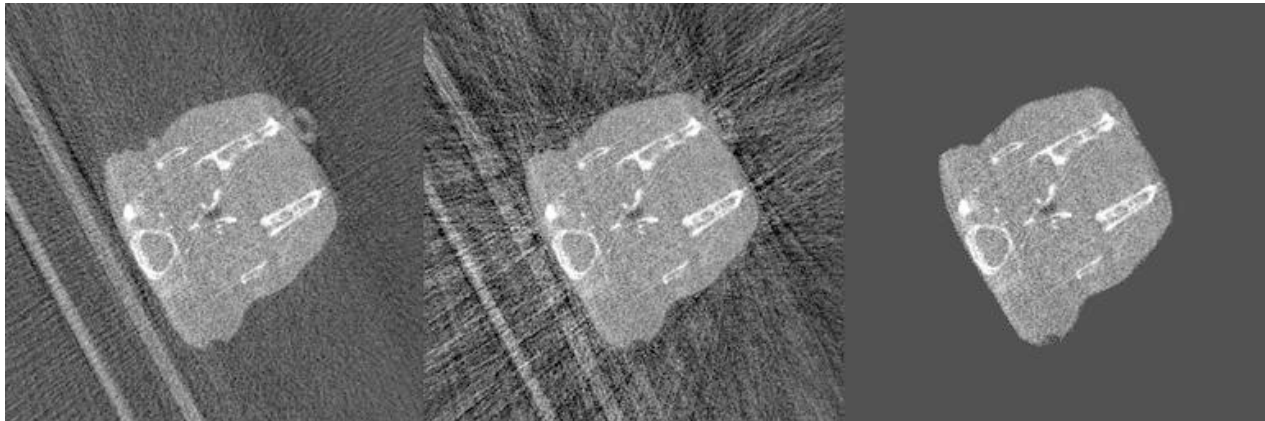


Figure 6. The standard reconstruction as a reference (right), the reconstruction of the volume of interest including the outside (middle), and only the volume of interest reconstruction (left).

## 5. DISCUSSION AND CONCLUSION

In this paper, we have presented an approach which gives any tomographic reconstruction algorithm the capability of reliable segmentation and identification of a volume of interest from a reduced number of projections. Our method rapidly identifies a volume of interest using active shape models as reconstructions proceed from a flexible number of projections. The volume of interest is subsequently reconstructed using the full projection set. By focusing on the region of interest, the reconstruction can be done more quickly and with improved statistics. An additional feature of our algorithm is that a segmentation of objects of interest is done after a small number of projections. Since a segmentation of the object of interest is possible after a small number of projections, the x-ray dose can be reduced. This is important, since with population dose increasing (in part due to dose imparted by more frequent recourse to CT), thus, new approaches must be developed to reduce the dose.

In our evaluations, we reported promising results on clinical and simulated data sets. For a two dimensional slice with dimensions 512 x 512, our algorithm returns after 10 sec. By using the full reconstruction as the “gold standard”, we performed a leave-one-out cross-validation and reported an average overlap accuracy of 91%.

## 6. ACKNOWLEDGEMENTS

This work was partly supported by The State University of New York at Buffalo - Interdisciplinary Research Development Fund, NSF grant IIS-0713489, NSF CAREER Award CCF-0546509, and the Toshiba Medical Systems Corporation.

## REFERENCES

- [1] Zhang, Y., Chan, H., Sahiner, B., Wei, J., Goodsitt, M., Hadjiiski, L., Ge, J., and Zhou, C., “A comparative study of limited-angle cone-beam reconstruction methods for breast tomosynthesis,” *Med Phys* **33**, 3781–3795 (Oct 2006).
- [2] Chen, G.-H., Siewerdsen, J. H., Leng, S., Moseley, D., Nett, B. E., Hsieh, J., Jaffray, D., and Mistretta, C. A., “Guidance for cone-beam ct design: tradeoff between view sampling rate and completeness of scanning trajectories,” *Medical Imaging 2006: Physics of Medical Imaging* **6142**(1), 614212, SPIE (2006).
- [3] Candes, E., Romberg, J., and Tao, T., “Robust uncertainty principles: exact signal reconstruction from highly incomplete frequency information,” *Information Theory, IEEE Transactions on* **52**(2), 489–509 (Feb. 2006).
- [4] Singh, V., Mukherjee, L., Dinu, P., Xu, J., and Hoffmann, K., “Limited view ct reconstruction and segmentation via constrained metric labeling,” *Comput. Vis. Image Underst.* **112**(1), 67–80 (2008).
- [5] Cootes, T. F., Taylor, C. J., Cooper, D. H., and Graham, J., “Active shape models - their training and application,” *Comput. Vis. Image Underst.* **61**(1), 38–59 (1995).
- [6] Feldkamp, L. A., Davis, L. C., and Kress, J. W., “Practical cone-beam algorithm,” *J. Opt. Soc. Am. A* **1**(6), 612 (1984).
- [7] Noël, P. B., Walczak, A. M., Hoffmann, K. R., Xu, J., Corso, J. J., and Schafer, S., “Clinical evaluation of gpu-based cone beam computed tomography,” *MICCAI Workshop: High-Performance Medical Image Computing and Computer Aided Intervention* (2008).
- [8] Schönemann, P. H., “A generalized solution of the orthogonal procrustes problem,” *Psychometrika* **31**(1) (1966).